Biomaterials 38 (2015) 43–49

Contents lists available at ScienceDirect

Biomaterials

journal homepage: www.elsevier.com/locate/biomaterials

Photo-induced inhibition of Alzheimer's β-amyloid aggregation in vitro by rose bengal

Joon Seok Lee [a, b], Byung Il Lee [a, b], Chan Beum Park [a, b, *]

[a] KAIST Institute for the BioCentury, Korea Advanced Institute of Science and Technology (KAIST), Daejeon 305-701, Republic of Korea
[b] Department of Materials Science and Engineering, Korea Advanced Institute of Science and Technology (KAIST), Daejeon 305-701, Republic of Korea

ARTICLE INFO

Article history:
Received 15 August 2014
Accepted 19 October 2014
Available online 11 November 2014

Keywords:
Peptide self-assembly
Beta-amyloid
Photosensitizers
Inhibitors
Rose bengal

ABSTRACT

The abnormal aggregation of β-amyloid (Aβ) peptides in the brain is a major pathological hallmark of Alzheimer's disease (AD). The suppression (or alteration) of Aβ aggregation is considered to be an attractive therapeutic intervention for treating AD. We report on visible light-induced inhibition of Aβ aggregation by xanthene dyes, which are widely used as biomolecule tracers and imaging markers for live cells. Among many xanthene dyes, rose bengal (RB) under green LED illumination exhibited a much stronger inhibition effect upon photo-excitation on Aβ aggregation than RB under dark conditions. We found that RB possesses high binding affinity to Aβ; it exhibits a remarkable red shift and a strong enhancement of fluorescence emission in the presence of Aβ. Photo-excited RB interfered with an early step in the pathway of Aβ self-assembly and suppressed the conformational transition of Aβ monomers into β-sheet-rich structures. Photo-excited RB is not only effective in the inhibition of Aβ aggregation, but also in the reduction of Aβ-induced cytotoxicity.

1. Introduction

Alzheimer's disease (AD) is the most common progressive neurodegenerative disease, affecting more than 13% of the population over age 65 [1]. The most prominent pathological hallmark observed in AD patients' brains is an abnormal accumulation of extracellular β-amyloid (Aβ) senile plaques [2]. An Aβ monomer, a polypeptide of 39–42 amino acids, is released after the sequential proteolytic cleavage of β-amyloid precursor proteins by β-and γ-secretases. Through nucleation-dependent polymerization, Aβ monomers either self-assemble into small, β-sheet-rich oligomers and protofibrils that are on-pathway intermediates to the formation of ordered amyloid fibrils, or transform into spherical, non-β-sheet oligomers related to off-pathway aggregation [3]. Various amyloid aggregate species are formed during the on/off-pathways, but their structures, sizes, and biological functions have not yet been clearly understood [3,4].

The suppression of Aβ aggregation (or the alteration of amyloid self-assembly pathways) is considered to be an attractive therapeutic intervention for treating AD [3]. In this paper, we report on visible light-induced inhibition of Aβ aggregation by photosensitizing molecules (Fig. 1a). Light is a clean, non-invasive, and inexpensive energy source that is useful for medicine (e.g., photodynamic [5–7] and photothermal therapies [8], and optogenetics [9–11]) as well as renewable energy development (e.g., solar cells [12], artificial photosynthesis [13]). For example, photodynamic therapy is a promising method for localized cancer treatment that utilizes a combination of photosensitizers and visible light to destroy tumor vessels and tissues by generating reactive oxygen species [5]. Optogenetics presents another example of medical utility of light, as it aims to control neural activity in the brain by optically stimulating light-sensitive proteins [9]. Recently, Deisseroth et al. recorded neural activity in a photoelectrochemical, artifact-free manner using laser-coupled optical fibers that were inserted directly into the brain of an animal, thus demonstrating the possibility of using light energy to determine the relationship between brain activity and behavior [10].

2. Materials and methods

2.1. Materials

Human $A\beta_{42}$ peptide was obtained from rPeptide (Bogart, GA) as lyophilized powder. Xanthene dyes and 2,4-dinitrophenylhydrazine (DNPH) were obtained from Sigma (St. Louis, MO). A11 antibody and horseradish peroxidase (HRP)-conjugated anti-rabbit IgG were purchased from Invitrogen. 6E10 antibody and HRP-

* Corresponding author. Department of Materials Science and Engineering, Korea Advanced Institute of Science and Technology (KAIST), Daejeon 305-701, Republic of Korea. Tel.: +82 42 350 3340; fax: +82 42 350 3310.
E-mail address: parkcb@kaist.ac.kr (C.B. Park).

http://dx.doi.org/10.1016/j.biomaterials.2014.10.058
0142-9612/

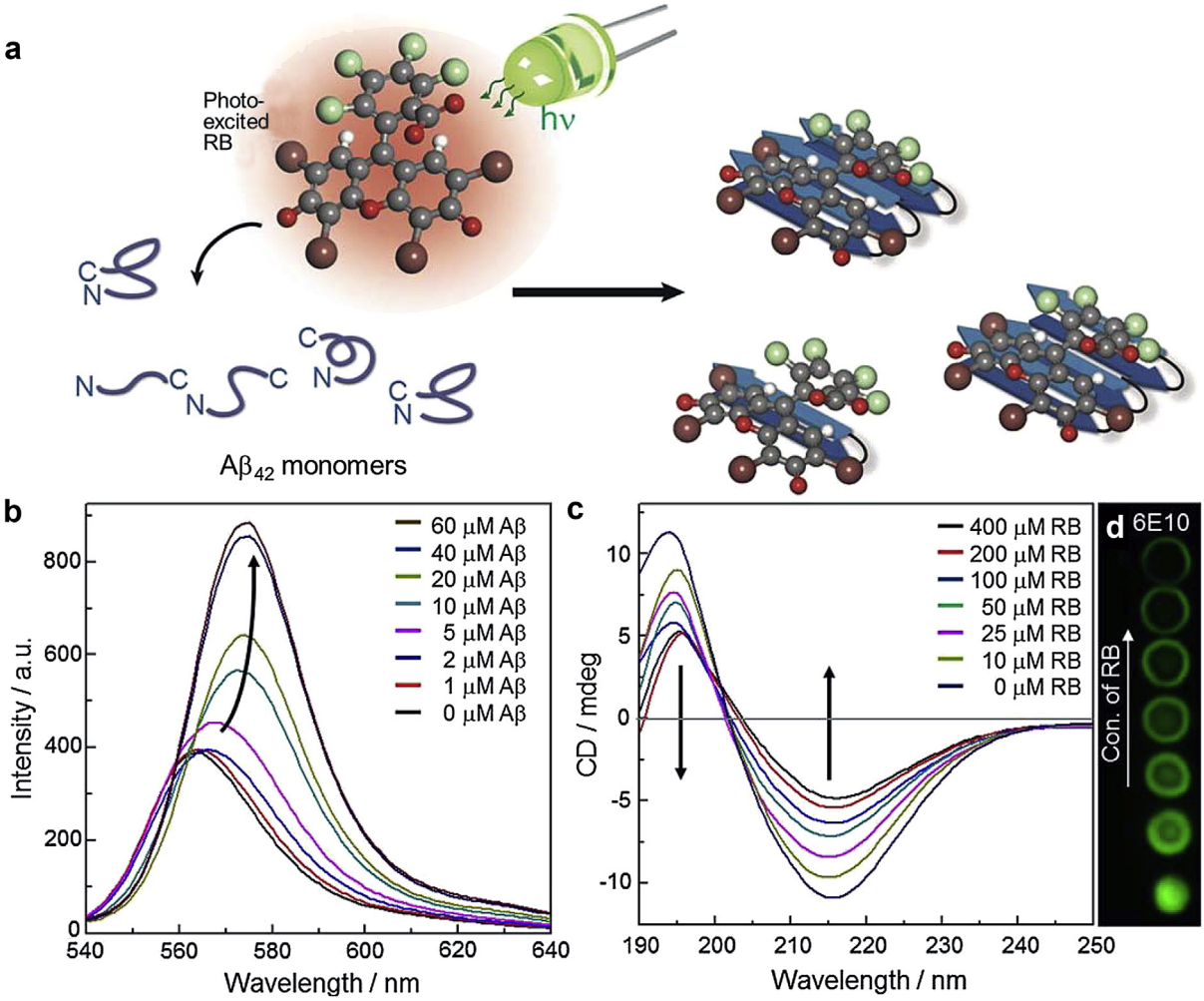

Fig. 1. (a) Schematic illustration of the inhibition of Aβ aggregation by photo-excited RB. (b) Fluorescence spectra of 1 μM RB in phosphate buffer upon addition of various concentrations of $A\beta_{42}$ peptide. (c), (d) CD spectra and dot blot of 40 μM $A\beta_{42}$ solutions incubated with various concentrations of RB under dark conditions during 24 h at 30 °C.

conjugated anti-mouse IgG were purchased from GenScript (Piscataway, NJ) and Promega (Madison, WI), respectively. 0.2-μm nitrocellulose membranes are available from Bio-rad (Richmond, CA). ECL chemiluminescence kit was from Amersham Biosciences (Piscataway, NJ).

2.2. Preparation of monomeric Aβ solution

1.0 mg of $A\beta_{42}$ was dissolved in hexafluoro-2-propanol (HFIP) by brief sonication for 1 min and kept overnight at room temperature. The solution was partitioned in protein Lobind microcentrifuge tubes (62.5 μg aliquots), and the HFIP was left to evaporate in a vacuum desiccator until lyophilized $A\beta_{42}$ film was visible. The resulting film was stored at −20 °C and used for further experiments. The $A\beta_{42}$ film was dissolved in a mixture (30 μL) that consisted of CH_3CN (300 μM)/Na_2CO_3 (300 μM)/NaOH (250 mM) (33.8:33.8:2.38, v/v/v), by brief sonication for 1 min. The monomeric $A\beta_{42}$ solution was diluted to a final concentration of 40 μM with a phosphate buffer (8.5 mM) that contained NaCl (8.5 mM), Na_2CO_3 (14 μM), NaOH (0.85 mM) and acetonitrile (6.0%; final pH 8.0) in the absence/presence of xanthene dyes.

2.3. Inhibition of Aβ aggregation under visible light irradiation

Red, green, and blue light-emitting diode (LED) lamps (Nichia Chem. Ind., Japan), a white LED lamp (Komabiotech, Korea), and a monochromator-coupled xenon lamp (Model 66924, Oriel, Irivine, CA) were used as light sources. The glass vials containing the prepared monomeric Aβ solution were exposed to visible light or covered with aluminum foil to exclude light, and then incubated for 24 h at 30 °C. The radiation intensity was measured using a Thorlabs PM100D optical power meter (Thorlabs Inc, Newton, NJ). The binding constant of RB was calculated by plotting the reciprocal of the fluorescence change at 572 nm against the $A\beta_{42}$ concentration with nonlinear fitting using Origin 8 software.

2.4. Circular dichroism (CD)

Far-UV CD spectra were measured using a JASCO J-810 (Jasco, Japan) spectropolarimeter at room temperature. To follow $A\beta_{42}$ conformational changes, the CD intensity of the 216 nm signal was plotted versus the time of incubation.

2.5. Dot blot assay

2 μL aliquots of each Aβ solution were applied to nitrocellulose membranes (Hybond ECL, GE healthcare). The membranes were blocked for 1 h at room temperature with 10% nonfat dry milk in Tris-buffered saline containing 0.01× tween 20 (TBST) and washed 3 times. The membranes were incubated with A11 or 6E10 antibodies diluted 1:500 to 1:1000 (5% nonfat dry milk in TBST). The membranes were washed again and incubated with the appropriated HRP-conjugated secondary antibody (goat-anti-rabbit for A11, goat-anti-mouse for 6E10). After washing, the blots were developed with the ECL chemiluminescence kit.

2.6. Native gel electrophoresis and silver staining

The Aβ solutions were transferred to a loading buffer containing 50 mM Tris HCl, pH 6.8, 10% (v/v) glycerol, and 0.01% bromophenol blue. The samples were loaded onto 10–20% tris-tricine gels (Biorad, Munich, Germany) without heat denaturation. $A\beta_{42}$ distribution in the native gels was visualized by silver staining.

2.7. AFM analysis

$A\beta_{42}$ samples were deposited on fresh cleaved mica and allowed to adsorb for 20 min. AFM images were acquired in a tapping mode in air with an NCHR silicon cantilever (Nanosensors Inc., Switzerland) by using a Multimode AFM instrument equipped with a Nanoscope III controller and "E"-type scanner (Digital Instruments Inc., Santa Barbara, CA).

2.8. MTT assay

PC12, a cell line derived from a rat pheochromocytoma, were cultured in RPMI 1640 media with 10% horse serum (HS), 5% fetal bovine serum (FBS) and 1% antibiotics. Cells were maintained in an atmosphere of 5% CO_2 at 37 °C and subcultured at least twice a week. The cells were seeded in a 96-well plate at a density of 2×10^4 cells in 100 μl and then incubated for 24 h for attachment to the bottom of the wells. We added the Aβ aggregates pre-formed in different conditions to well plates (1% final concentration) and incubated them under 5% CO_2 atmosphere at 37 °C. For the observation of cellular effect of singlet oxygen generated by photo-induced RB in the presence of Aβ in comparison with the effect on the modulation of Aβ aggregation, we added samples (1, 5, and 10% of the final volume in 100 μl culture medium) containing fresh Aβ monomers and RB and illuminated green LED on the well plates during the cell culture process. We completely removed culture medium containing Aβ and RB after cell culture for 24 h and replaced the medium with 10 μl of 5 mg/ml MTT solution and 90 μl of fresh culture medium, and then the cells were further incubated for additional 3 h. The resulting formazan (purple colored product) was dissolved in 100 μl of DMSO, and the absorbance was measured at 595 nm using a Victor 3 microplate reader (PerkinElmer Inc., MA, U.S.A.). All the error bars from MTT assays represent standard deviation of at least three different experiments. Statistical analysis was carried out by means of one-way analysis of variance (ANOVA).

2.9. DNPH assay

Aβ solutions with or without RB were precipitated using trichloroacetic acid (TCA, 20% final concentration). We added a solution of 2 N HCl containing DNPH (10 mM) to the precipitated Aβ pellets. After 1 h, the pellets were first washed with 20% TCA solution and then washed three times using ethanol/ethyl acetate (1:1, v/v) solution. The samples were resuspended in a guanidine hydrochloride solution (6 M, pH 2.3) at 37 °C. The absorbance spectrum of the samples was measured using a V/650 spectrophotometer (Jasco Inc., Japan).

3. Results and discussion

3.1. Screening of xanthene dyes under dark for inhibition of Aβ aggregation

We investigated possible photo-induced inhibition of Aβ aggregation by xanthene dyes (see Fig. S1 for their chemical structures) that are widely used as tracers for biomolecules and imaging markers for live cells [14]. In order to test the effect of xanthene dyes on Aβ aggregation, we observed the binding interaction between each dye and $A\beta_{42}$ peptide under dark conditions. Among xanthene dyes, rose bengal (RB) exhibited a remarkable red shift ($\Delta\lambda = 12$ nm) and a strong enhancement of fluorescence emission in the presence of $A\beta_{42}$ (Fig. S2), which indicates strong association between RB and $A\beta_{42}$. This fluorescence enhancement is attributed to the reduction in the non-radiative decay of photo-excited RB due to the restricted vibration and rotation of RB in the presence of $A\beta_{42}$ [15–18]. To determine the binding affinity of RB with $A\beta_{42}$, we evaluated fluorescence intensity changes at 574 nm at different RB/$A\beta_{42}$ ratios (Fig. 1b, Fig. S3). The binding constant (K_d) of RB to $A\beta_{42}$ was estimated to be approximately 17 μM. Note that small molecules with high-affinity binding to Aβ (e.g., K_d of thioflavin $T = 0.7 \sim 1$ μM, K_d of curcumin = 5 μM) [19–21] have been widely used as markers and inhibitors for Aβ aggregation. The results indicate that RB has high binding affinity to $A\beta_{42}$. The RB interaction with $A\beta_{42}$ was also evident from the red shift of absorbance spectrum (550 nm → 562 nm) with the increasing concentration of $A\beta_{42}$ (Fig. S4). According to the literature [13], the absorption of RB in the spectrum range originates from $n-\pi^*$ transitions and the shift of RB absorbance spectrum occurs when RB chromophore exists in more nonpolar environment upon binding. When RB was mixed with $A\beta_{42}$ aggregates or monomers, both mixtures exhibited same red shift of absorbance and fluorescence spectra (Fig. S5).

We conducted circular dichroism (CD) analysis to examine whether xanthene dyes affect $A\beta_{42}$ aggregation. CD analysis has been routinely used to analyze amyloid aggregation [22], a process that offers real-time monitoring of conformational states and secondary structure transitions of $A\beta_{42}$ in aqueous solutions. After incubation in the absence of xanthene dye at 30 °C for 24 h, $A\beta_{42}$ exhibited a minimum at 216 nm and a maximum at 197 nm, which indicates typical conversion of $A\beta_{42}$ monomers and small aggregates into β-sheet-rich aggregates (Fig. S6). The addition of xanthene dyes resulted in drastic changes of CD spectra, as shown in Fig. S7. Note that the dyes did not exhibit any CD spectrum peak in the UV range irrespective of light illumination (Fig. S8). In the case of fluorescein, eosin B, rhodamine B, and sulforhodamine B, absolute CD values at 216 nm is similar to that of only $A\beta_{42}$, which indicates the dyes had negligible effects on the formation of β-sheet-rich $A\beta_{42}$ aggregates. However RB, ethyleosin, eosin Y, and phloxine B, which have structures of xanthene benzoate group attached to different halogen atoms, exhibited much stronger inhibition effects (Fig. S1,S7,S8). According to the literature [23–26], halogenation of aromatic molecules significantly affects aromatic interaction-mediated self-assembly processes, including Aβ aggregation and cytotoxicity. For example, Wong and Kwon reported that erythrosine B, a xanthene dye, can modulate $A\beta_{40}$ aggregation [27]. Note that competitive interaction between aromatic residues is attributed to the formation of β-sheet rich Aβ structures [28]. The perturbation of the aromatic interaction caused by halogenation of peptide building blocks plays a critical role in affecting the morphology and physical properties of aggregated Aβ structure [24,25]. In particular, RB exhibited the highest degree of inhibition. These results imply that the interaction between RB and $A\beta_{42}$ hinders the self-assembly of $A\beta_{42}$ monomers, a finding that is consistent with the results of the fluorescence and absorption spectroscopic analyses. Fig. 1c shows CD spectrum profiles of $A\beta_{42}$ (40 μM) in the presence of RB at different concentrations (0 ~ 400 μM). According to the CD data, RB inhibited $A\beta_{42}$ aggregation at stoichiometric concentrations relative to the $A\beta_{42}$ monomer concentration. We conducted dot blotting assays using a 6E10 antibody, an Aβ-sequence-specific monoclonal antibody that binds to the residues 1–16 of $A\beta_{42}$ (Fig. 1d). With increasing concentrations of RB, 6E10-immunoreactivity of $A\beta_{42}$ became significantly weaker than that which was observed in the absence of RB. This result implies that RB may limit the accessibility of the antibody to the 6E10 epitope of $A\beta_{42}$, suggesting possible inhibition of on-pathway $A\beta_{42}$ aggregation by RB.

3.2. Photo-excited RB exhibits strong inhibition of Aβ aggregation

Under light irradiation, RB exhibits a strong absorption band at around 550 nm and a high quantum yield of triplet state formation [18]. To examine the effect of photo-excited RB on Aβ aggregation, we incubated $A\beta_{42}$ and RB together under the illumination of a white light-emitting diode (LED) (Fig. 2a). According to a recent report [11], LED is a promising photo-device for wireless and programmed behavioral control of freely moving animals, as it can operate in a minimally invasive way in the soft tissues of mammalian brains. In the absence of RB, the CD spectrum was identical to those obtained under dark conditions (Fig. 2b and Fig. S9), and numerous, fully grown Aβ fibrils were observed according to *ex situ* AFM analysis (Fig. 2c), which indicates that visible light irradiation on $A\beta_{42}$ alone does not affect its aggregation. We attribute the unusually large aggregates among the globular aggregates to possible formation of RB aggregates. Upon light illumination, photo-excited RB exhibited much greater inhibitory effects on $A\beta_{42}$ aggregation than it did under dark conditions. The minimum at 216 nm of CD spectra was significantly reduced—similar to the spectrum of unstructured—native $A\beta_{42}$ monomers, and only small aggregates of globular morphology were observed (Fig. 2c). Fig. S10 shows the effect of various xanthene dyes under light illumination on Aβ aggregation, which shows that RB exhibited the highest degree of inhibition among the dyes. To investigate the effect of photo-excited RB on immunoreactivity and

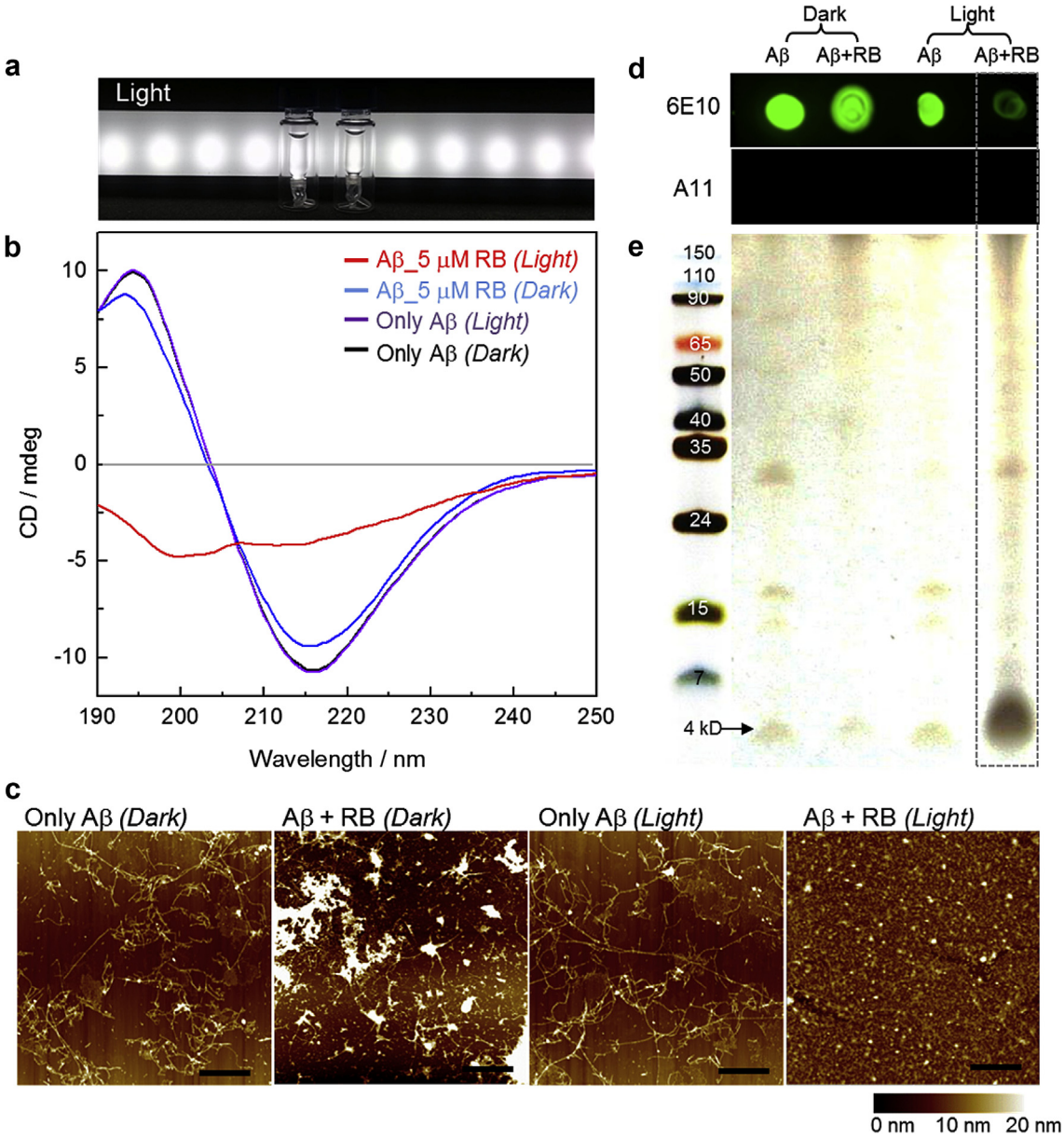

Fig. 2. (a) An experimental photograph of $A\beta_{42}$ solution with/without RB illuminated by a white light LED. Analysis of photo-induced inhibition on Aβ aggregation by (b) CD spectroscopy, (c) AFM, (d) Dot blotting, and (e) Native gel electrophoresis and silver staining. $A\beta_{42}$ (40 μM) was incubated with/without RB (5 μM) under dark conditions or white LED light at 30 °C during 24 h. Scale bars 2 μm.

size changes of $A\beta_{42}$ aggregates, we performed dot blotting assays and native gel electrophoresis. The dot blotting assay result shows that photo-excited RB significantly decreases 6E10-immunoreactivity of $A\beta_{42}$ aggregates (Fig. 2d). The dyes (e.g., sulforhodamine B, eosin B) not interacting with $A\beta_{42}$ exhibited no effect on signal intensity of dot blotting (Fig. S11). This result implies that RB limits the antibody accessibility much more strongly under light irradiation to the epitope of 6E10 antibody. In the case of dot blotting analysis with an A11 antibody—a polyclonal antibody that only recognizes toxic, globular Aβ oligomeric structures, not monomers or fibrils [29]—we could not observe any signal for any of the four dots of $A\beta_{42}$ aggregates formed without RB (dark/light) or with RB (dark/light). The lack of dot signal with the A11 antibody indicates that the small, globular $A\beta_{42}$ aggregates shown in Fig. 2c are conformationally distinct from the epitope of the A11 antibody [30]. According to native gel electrophoresis analysis of $A\beta_{42}$ aggregates formed without RB (dark/light) and with RB (dark ONLY), we could observe very weak bands for monomers (~4 kD), small oligomers (15–20 kD and 35 kD), and medium-size oligomers (40–150 kD) (Fig. 2e), which result is attributed to the assembly of most $A\beta_{42}$ monomers into fibrils (Fig. 2c) [4]. In the presence of RB under light irradiation, however, the intensity of the monomer band (~4 kD) became much stronger. These results show that photo-excited RB inhibits $A\beta_{42}$ aggregation significantly.

3.3. Effect of RB concentration, light wavelength, and energy density on Aβ aggregation

We investigated photo-excited RB's inhibition of $A\beta_{42}$ aggregation by changing RB concentration, light wavelength, and energy density. The increased concentration of RB caused a higher inhibition degree of $A\beta_{42}$ aggregation only under light irradiation according to our CD analysis (Fig. 3a, b). Photo-excited RB exhibited much stronger inhibitory effect on $A\beta_{42}$ aggregation than RB under

dark conditions. We also observed the effect of incident light wavelengths using red, green, and blue LEDs. Under the irradiation with the red LED, amyloid aggregation was negligibly inhibited according to CD and AFM analyses (Fig. 3d, e), which was similar to the effect of RB under dark. In contrast, under blue and green LEDs, significant changes in CD spectrum were observed with the appearance of small, globular aggregates rather than fibrils. These results are attributed to the discrepancy between the photon energy emitted by each LED and that absorbed by RB; RB can absorb photon energy levels of 2.06 ~ 2.75 eV while each LED possesses the following energy band: 1.84 ~ 2.16 eV (red), 2.03 ~ 2.69 eV (green), and 2.29 ~ 2.75 eV (blue) (Fig. 3c). When we changed the power density of green LED (0 ~ 20 mW/cm^2), more suppression of Aβ_{42} aggregation was observed with the increasing energy power in the presence of RB (Fig. S12, S13). When we incubated a mixture of Aβ and RB under irradiation of white LED light for 12 h followed by incubation for another 12 h under dark condition, we observed similar inhibition effect as in the light irradiation for full 24 h (Fig. S14). This result indicates that continuous illumination of light is not needed for photo-induced Aβ aggregation. We may further shorten the illumination time by controlling dye concentration and light intensity (Fig. 3a, Fig. S13). We further observed the kinetics of photo-induced inhibition of Aβ_{42} aggregation using a monochromator-coupled xenon lamp at 514 nm, the maximum absorption wavelength of RB (Figs. S15, S16). Fig. S16e shows time profiles of absolute CD value at 216 nm recorded during the

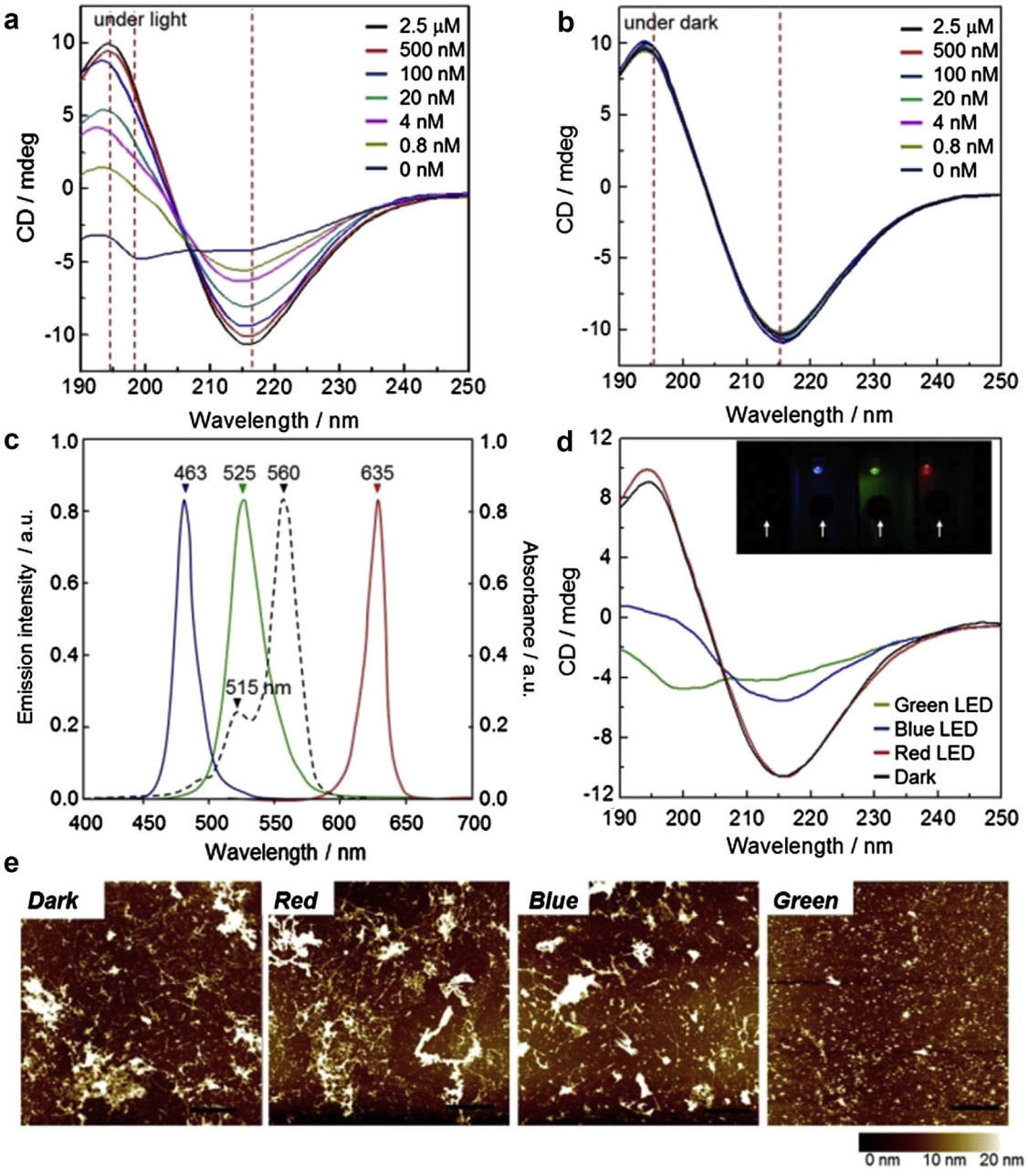

Fig. 3. Effect of various light sources in the presence of RB on Aβ aggregation. (a) and (b) CD spectra of Aβ_{42} solutions incubated in the presence of various concentrations of RB under light and dark. (c) Absorbance spectrum of RB in phosphate buffer and emission spectra of red, green, and blue LEDs. (d) CD spectra (insert: image of red, green, and blue LEDs) and (e) AFM images of Aβ_{42} solutions in the presence of RB under the LEDs illumination. Scale bars 2 μm. (For interpretation of the references to color in this figure legend, the reader is referred to the web version of this article.)

incubation of $A\beta_{42}$ monomers. In the case of $A\beta_{42}$ incubated in the absence of RB under dark and light, we observed a sigmoidal curve that is characterized by three steps: a lag phase, an exponential growth phase, and a plateau phase. In contrast, with the irradiation of monochromatic light at 514 nm in the presence of RB, no change of absolute CD value at 216 nm was observed with prolonged lag phase only. This result indicates that photo-excited RB interferes with a very early step in the $A\beta_{42}$ self-assembly pathway, suppressing the conformational transition of $A\beta_{42}$ monomers and small aggregates into β-sheet-rich structures.

We attribute the inhibition of $A\beta_{42}$ aggregation by photo-excited RB to a binding affinity of RB to $A\beta_{42}$, the vibration of photo-excited RB, and the photo-oxidation of $A\beta_{42}$ residues. Our data obtained using CD, absorption and fluorescence spectroscopies, and dot blotting assay indicate that RB has an affinity to $A\beta_{42}$ and inhibits its conversion into β-sheet-rich structures. Since photo-active dyes release ROS, vibration, electric, or photon energies upon excitation by light, the binding of dye molecules on a certain biological level, such as DNA and peptides, can reduce skeleton vibration of the dye and facilitate the transfer of excitation energy, leading to the fluorescence enhancement of the dye molecules [15,18,31]. The vibration of the excited dye continues under maintained light irradiation in contrast to static dye under dark; thus, the vibration of photo-excited RB bound with $A\beta_{42}$ would interfere with the coalescence of $A\beta_{42}$ monomers. Fig. S17 shows absorbance spectra of RB in the presence of $A\beta_{42}$ after dark and light illumination. Photo-excited RB in the presence of $A\beta_{42}$ was significantly degraded during light illumination [32]. In addition, RB that was pre-illuminated for 24 h did not influence Aβ aggregation, indicating that photo-degraded RB has negligible inhibitory effect on Aβ aggregation (Fig. S18). Considering that photosensitizers cause photo-induced damage of proteins upon the absorption of visible light [33], RB should induce photo-oxidation of $A\beta_{42}$ under green light illumination. Fig. S19 shows the effect of photo-excited RB under anaerobic condition (i.e., Ar-saturated buffer containing 2 mM sodium azide as a singlet oxygen quencher) [34,35] on Aβ aggregation. The degree of inhibition under anaerobic condition was decreased significantly in comparison with that under aerobic condition (see Fig. 3a or Fig. S19b). We further conducted 2,4-dinitrophenylhydrazine (DNPH)-based assay, which is a highly sensitive method for the observation of protein oxidation (Fig. S20). In the case of Aβ incubated in the presence of photo-excited RB, new absorption peak was clearly observed at around 370 nm, corresponding to the reaction of the carbonyl group of oxidized Aβ with DNPH. Note that RB is frequently employed as sensitizer for photodynamic therapy due to its high singlet oxygen quantum yield, high water solubility, and its low rate of photodegradation [36–38]. According to the literature [33,39–41], a ground state RB was boosted into a high-energy state by the absorption of visible light, which generates singlet oxygen ($^1O_2$) by energy transfer to O_2, leading to photo-induced damage of neighboring proteins through the formation of reactive intermediates between amino acid residues (e.g., His, Tyr, Phe) and $^1O_2$. Therefore, singlet oxygen generated from photo-excited RB directly modulates Aβ aggregation. Based on the photochemical property of RB, we speculate that photo-induced damage of $A\beta_{42}$ in the presence of RB under light illumination would preclude the self-assembly of $A\beta_{42}$ peptides into on-pathway aggregates.

3.4. Photo-excited RB influences $A\beta_{42}$ cytotoxicity

We tested the viability of PC12 cells using a 3-(4,5-dimethylthiazol-2yl)-2,5-diphenyltetrazolium bromide (MTT) assay [42]. As shown in Fig. S21a, the effect of RB in the concentration range of 0.02–10 μM was negligible on MTT assay under dark condition. Fig. 4a shows relative numbers of live cells incubated with $A\beta_{42}$ aggregates formed with or without RB under dark and light conditions. We observed a high toxicity of $A\beta_{42}$ aggregates assembled in the presence of RB under dark. In contrast, cell viability was noticeably increased when $A\beta_{42}$ was incubated with RB under green LED illumination. Photo-excited RB exhibited an inhibitory effect on cytotoxic Aβ aggregation with an IC_{50} value of approximately 0.4 μM (Fig. S21b, c). We further observed the effect of singlet oxygen production by photo-induced RB on cells in comparison with the effect on the modulation of Aβ aggregation (Fig. 4b). Singlet oxygen generated from photo-excited RB under the illumination exhibited negligible effect on cell viability in contrast to the modulation of cytotoxic Aβ aggregation. This result indicates that photo-excited RB is not only effective in *in vitro* inhibition of $A\beta_{42}$ aggregation, but also in the reduction of $A\beta_{42}$-

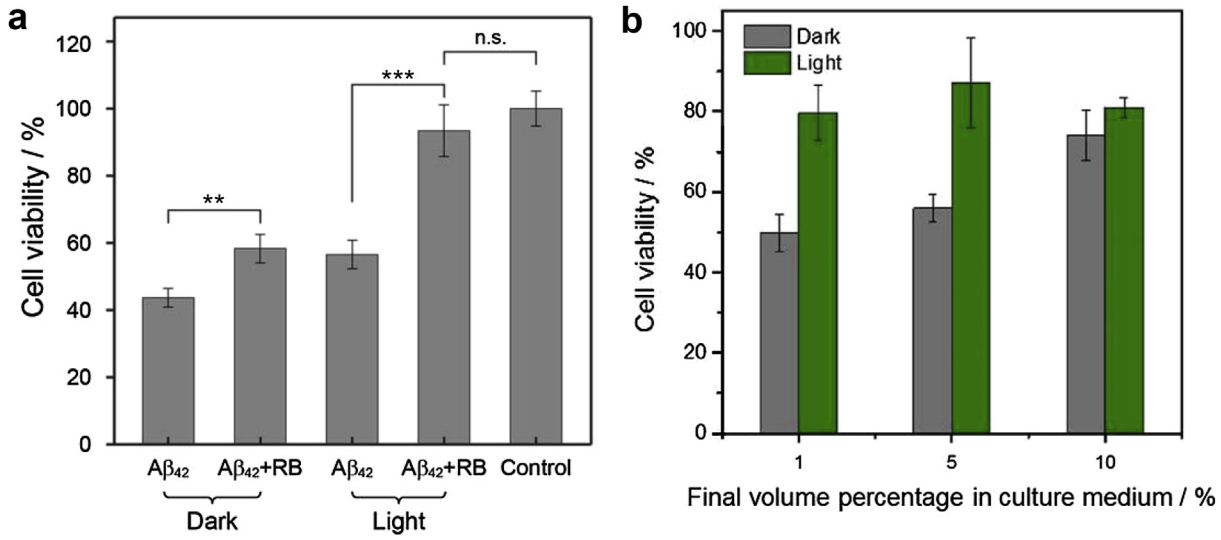

Fig. 4. (a) Cytotoxicity assays of $A\beta_{42}$ aggregates formed without RB (dark/light) and with RB (dark/light) against PC12 cells using the MTT method. ($n = 6$, $^{**}p < 0.005$, $^{***}p < 0.001$) (b) Cytotoxicity of cells cultured with Aβ and RB under light illumination, which shows negligible cytotoxic effect of singlet oxygens generated by photo-excited RB on cells, in contrast to the effect of photo-induced modulation of Aβ aggregation. For this experiment, sample solution (1, 5, and 10% of final volume in 100 μl culture medium) containing fresh Aβ monomers (40 μM) with RB (2.5 μM) were added to the well plate containing PC12 cells, then green LED was illuminated on the well plate during cell culture. All the error bars from MTT assays represent standard deviation of at least three different experiments. (For interpretation of the references to color in this figure legend, the reader is referred to the web version of this article.)

induced cytotoxicity. Further studies are needed for *in vivo* applications through the design and optimization of photosensitizing molecules and photo-irradiation system.

4. Conclusion

RB strongly inhibits Alzheimer's $A\beta_{42}$ aggregation upon its absorption of visible light energy (2.06 ~ 2.75 eV). We observed significant red shift ($\Delta\lambda$ = 12 nm) and strong enhancement of fluorescence emission of RB in the presence of $A\beta_{42}$. Photo-excited RB exhibited much stronger inhibitory effect on $A\beta_{42}$ aggregation than RB under dark conditions. RB exhibited the relatively higher binding affinity to $A\beta_{42}$ than other xanthene dyes and reduced the accessibility of the 6E10 antibody to the epitope of $A\beta_{42}$. RB under green LED illumination interfered with an early step in the pathway of $A\beta_{42}$ self-assembly and inhibited the conformational transition of $A\beta_{42}$ monomers into β-sheet-rich structures. This photo-induced inhibition is attributed to the interaction between RB and $A\beta_{42}$ peptides, the vibration of photo-excited RB, and photo-oxidation of $A\beta_{42}$. An effect of photo-excited RB against the cytotoxicity of $A\beta_{42}$ towards PC12 cells was also confirmed *in vitro*. This report hints at the potential of utilizing photo-excited dye molecules for effective suppression of Aβ aggregation and cytotoxicity.

Acknowledgments

This study was supported by grants from the National Research Foundation (NRF) via the National Leading Research Laboratory (NRF-2013R1A2A1A05005468) and the Intelligent Synthetic Biology Center of Global Frontier R&D Project (2011-0031957), Republic of Korea.

Appendix A. Supplementary data

Supplementary data related to this article can be found at http://dx.doi.org/10.1016/j.biomaterials.2014.10.058.

References

[1] Alzheimer's Association. 2012 Alzheimer's disease facts and figures. Alzheimers Dement 2012;8:131–68.
[2] Murphy RM. Peptide aggregation in neurodegenerative disease. Annu Rev Biomed Eng 2002;4:155–74.
[3] Ladiwala ARA, Dordick JS, Tessier PM. Aromatic small molecules remodel toxic soluble oligomers of amyloid beta through three independent pathways. J Biol Chem 2011;286:3209–18.
[4] Bieschke J, Herbst M, Wiglenda T, Friedrich RP, Boeddrich A, Schiele F, et al. Small-molecule conversion of toxic oligomers to nontoxic beta-sheet-rich amyloid fibrils. Nat Chem Biol 2012;8:93–101.
[5] Liang X, Li X, Jing L, Yue X, Dai Z. Theranostic porphyrin dyad nanoparticles for magnetic resonance imaging guided photodynamic therapy. Biomaterials 2014;35:6379–88.
[6] Vankayala R, Lin C, Kalluru P, Chiang C, Hwang KC. Gold nanoshells-mediated bimodal photodynamic and photothermal cancer treatment using ultra-low doses of near infra-red light. Biomaterials 2014;35:5527–38.
[7] Kuo WS, Chang CN, Chang YT, Yang MH, Chien YH, Chen SJ, et al. Gold nanorods in photodynamic therapy, as hyperthermia agents, and in near-infrared optical imaging. Angew Chem Int Ed 2010;49:2711–5.
[8] Gollavelli G, Ling Y. Magnetic and fluorescent graphene for dual modal imaging and single light induced photothermal and photodynamic therapy of cancer cells. Biomaterials 2014;35:4499–507.
[9] Fenno L, Yizhar O, Deisseroth K. The development and application of optogenetics. Annu Rev Neurosci 2011;34:389–412.
[10] Zhang F, Gradinaru V, Adamantidis AR, Durand R, Airan RD, de Lecea L, et al. Optogenetic interrogation of neural circuits: technology for probing mammalian brain structures. Nat Protoc 2010;5:439–56.
[11] T-i Kim, McCall JG, Jung YH, Huang X, Siuda ER, Li Y, et al. Injectable, cellular-scale optoelectronics with applications for wireless optogenetics. Science 2013;340:211–6.
[12] Feng XJ, Zhu K, Frank AJ, Grimes CA, Mallouk TE. Rapid charge transport in dye-sensitized solar cells made from vertically aligned single-crystal rutile TiO_2 nanowires. Angew Chem Int Ed 2012;51:2727–30.
[13] Lee SH, Kim JH, Park CB. Coupling photocatalysis and redox biocatalysis toward biocatalyzed artificial photosynthesis. Chem Eur J 2013;19:4392–406.
[14] Lee SH, Nam DH, Park CB. Screening xanthene dyes for visible light-driven nicotinamide adenine dinucleotide regeneration and photoenzymatic synthesis. Adv Synth Catal 2009;351:2589–94.
[15] Zhu M, Rajamani S, Kaylor J, Han S, Zhou FM, Fink AL. The flavonoid baicalein inhibits fibrillation of alpha-synuclein and disaggregates existing fibrils. J Biol Chem 2004;279:26846–57.
[16] Yang W, Wong Y, Ng OT, Bai LP, Kwong DW, Ke Y, et al. Inhibition of beta-amyloid peptide aggregation by multifunctional carbazole-based fluorophores. Angew Chem Int Ed 2012;51:1804–10.
[17] Cook NP, Kilpatrick K, Segatori L, Martí AA. Detection of α-synuclein amyloidogenic aggregates in vitro and in cells using light-switching dipyridophenazine ruthenium(II) complexes. J Am Chem Soc 2012;134:20776–82.
[18] Khajehpour M, Troxler T, Vanderkool JM. Probing the active site of trypsin with rose bengal: insights into the photodynamic inactivation of the enzyme. Photochem Photobiol 2004;80:359–65.
[19] Yona RL, Mazeres S, Faller P, Gras E. Thioflavin derivatives as markers for amyloid-beta fibrils: insights into structural features important for high-affinity binding. Chemmedchem 2008;3:63–6.
[20] Lockhart A, Ye L, Judd DB, Merritt AT, Lowe PN, Morgenstern JL, et al. Evidence for the presence of three distinct binding sites for the thioflavin T class of Alzheimer's disease PET imaging agents on beta-amyloid peptide fibrils. J Biol Chem 2005;280:7677–84.
[21] Pedersen MO, Mikkelsen K, Behrens MA, Pedersen JS, Enghild JJ, Skrydstrup T, et al. NMR reveals two-step association of congo red to amyloid beta in low-molecular-weight aggregates. J Phys Chem B 2010;114:16003–10.
[22] Bartolini M, Bertucci C, Bolognesi ML, Cavalli A, Melchiorre C, Andrisano V. Insight into the kinetic of amyloid beta(1-42) peptide self-aggregation: elucidation of inhibitors' mechanism of action. Chembiochem 2007;8:2152–61.
[23] Gazit E. A possible role for pi-stacking in the self-assembly of amyloid fibrils. Faseb J 2002;16:77–83.
[24] Wong HE, Irwin JA, Kwon I. Halogenation generates effective modulators of amyloid-beta aggregation and neurotoxicity. Plos One 2013;8:e57288.
[25] Nowak MW, Gallivan JP, Silverman SK, Labarca CG, Dougherty DA, Lester HA. In vivo incorporation of unnatural amino acids into ion channels in xenopus oocyte expression system. Method Enzymol 1998;293:504–29.
[26] Azriel R, Gazit E. Analysis of the structural and functional elements of the minimal active fragment of islet amyloid polypeptide (IAPP) – an experimental support for the key role of the phenylalanine residue in amyloid formation. J Biol Chem 2001;276:34156–61.
[27] Edward Wong H, Kwon I. Xanthene food dye as a modulator of Alzheimer's disease amyloid-beta peptide aggregation and the associated impaired neuronal cell function. Plos One 2011;6:e25752.
[28] Cheng B, Gong H, Xiao H, Petersen RB, Zheng L, Huang K. Inhibiting toxic aggregation of amyloidogenic proteins: a therapeutic strategy for protein misfolding diseases. Biochim Biophys Acta 2013;1830:4860–71.
[29] Hu Y, Su B, Kim C-S, Hernandez M, Rostagno A, Ghiso J, et al. A strategy for designing a peptide probe for detection of β-amyloid oligomers. Chembiochem 2010;11:2409–18.
[30] Ehrnhoefer DE, Bieschke J, Boeddrich A, Herbst M, Masino L, Lurz R, et al. EGCG redirects amyloidogenic polypeptides into unstructured, off-pathway oligomers. Nat Struct Mol Biol 2008;15:558–66.
[31] Ghosh JK, Mandal AK, Pal MK. Energy transfer from thiacyanine to acridine orange facilitated by DNA. Spectrochim Acta A 1999;55:1877–86.
[32] Xie YB, Yuan CW. Visible-light responsive cerium ion modified titania sol and nanocrystallites for X-3B dye photodegradation. Appl Catal B-Environ 2003;46:251–9.
[33] Pattison DI, Rahmanto AS, Davies MJ. Photo-oxidation of proteins. Photochem Photobiol Sci 2012;11:38–53.
[34] Misra BR, Misra HP. Vasoactive-intestinal-peptide, a singlet oxygen quencher. J Biol Chem 1990;265:15371–4.
[35] Miller JS. Rose bengal-sensitized photooxidation of 2-chlorophenol in water using solar simulated. Water Res 2005;39:412–22.
[36] Alarcon E, Edwards AM, Aspee A, Borsarelli CD, Lissi EA. Photophysics and photochemistry of rose bengal bound to human serum albumin. Photochem Photobiol Sci 2009;8:933–43.
[37] Zhang Y, Görner H. Photoprocesses of xanthene dyes bound to lysozyme or serum albumin. Photochem Photobiol 2009;85:677–85.
[38] Kishore S, Maruthamuthu M. Binding of rose-Bengal onto bovine serum-albumin. P Indian as-Chem Sci 1993;105:279–85.
[39] Chouikrat R, Seve A, Vanderesse R, Benachour H, Barberi-Heyob M, Richeter S, et al. Non polymeric nanoparticles for photodynamic therapy applications: recent developments. Curr Med Chem 2012;19:781–92.
[40] Posadaz A, Biasutti A, Casale C, Sanz J, Amat-Guerri F, García NA. Rose bengal-sensitized photooxidation of the dipeptides l-tryptophyl-l-phenylalanine, l-tryptophyl-l-tyrosine and l-tryptophyl-l-tryptophan: kinetics, mechanism and photoproducts. Photochem Photobiol 2004;80:132–8.
[41] Ozawa D, Kaji Y, Yagi H, Sakurai K, Kawakami T, Naiki H, et al. Destruction of amyloid fibrils of keratoepithelin peptides by laser irradiation coupled with amyloid-specific thioflavin. J Biol Chem 2011;286:10856–63.
[42] Geng J, Li M, Ren JS, Wang EB, Qu XG. Polyoxometalates as inhibitors of the aggregation of amyloid beta peptides associated with Alzheimer's disease. Angew Chem Int Ed 2011;50:4184–8.